Chapter 36
Research on Dynamic Condition Test of Power Battery Simulation Based on Principal Component Analysis

Hong Pei Li and Guixiong Liu

Abstract In this paper, the vehicle driving conditions used to measure gas emissions and the test conditions of power battery in simulated electric vehicle driving are divided into segments and feature extraction. Through the principal component analysis method, the principal components in the two working conditions are compared and analysed. Select the test condition data US06 of the power battery corresponding to the vehicle driving condition data, compare the characteristic parameters of the two conditions, and analyse the influence of the characteristic parameters of the working conditions on the power battery model. A voltage simulation model is established to detect the key parameters of the test battery. Finally, it is concluded that the state transition frequency is positively correlated with the simulation voltage accuracy of the power battery model in the test condition of the simulated electric vehicle.

36.1 Introduction

At the same time, electric vehicles are driven in ambient temperature changes, power demand changes in a wide range and high frequency of operating conditions, which brings greater difficulties for power battery model construction, parameter estimation and testing. The working condition method is the first experimental method to evaluate the emission status and economy of traditional vehicles [1], and distinguish the test of light vehicles and heavy vehicles. GB/T 38146.1-2019 *China Vehicle Driving Conditions Part 1: Light Duty Vehicles* [2] and GB/T 38146.2-2019 *China Vehicle Driving Conditions Part 2: Heavy Duty Commercial Vehicles* [3] provide the latest standards to suit the driving conditions of domestic vehicles.

GB/T 31467.2-2015 *Lithium-ion Power Battery Packs and Systems for Electric Vehicles Part 2 Test Procedure for High Energy Applications* [4] provides for the simulation of working conditions discharge and charging constant charge/discharge

H. P. Li · G. Liu (✉)
School of Mechanical and Automotive Engineering, South China University of Technology, Tianhe, Guangzhou, Guangdong, China
e-mail: megxliu@scut.edu.cn

G. Liu and F. Cen (eds.), *Advances in Precision Instruments and Optical Engineering*, Springer Proceedings in Physics 270, https://doi.org/10.1007/978-981-16-7258-3_36

test methods for power batteries. The test method is to test the power battery cells for cyclic constant current conditions.

However, in the course of road driving, electric vehicles are affected by the environment and work under the transition of starting, accelerating, braking, maintaining relatively constant speed and idling conditions. The battery modules and cells in the power battery system are regulated by electrical excitation and battery balancing management, and work under cyclic transformations of randomly varying currents for discharge and energy recovery [5]. The model construction and evaluation of key parameters of the power battery under dynamic operating conditions requires the use of simulated operating conditions for relevant tests [6, 7].

Depending on the road conditions and driver habits of each country [8], different driving conditions are constructed, and the variability of the discharge and energy recovery characteristics of the battery cells, modules and systems are also different after transformation by the EV simulation software [9, 10].

36.2 Battery Simulation Data Selection and Segmentation

36.2.1 Battery Simulation Data Selection

The power battery simulated working condition discharge and energy recovery power-time schedule mainly consists of two types: (1) vehicle simulation software, input vehicle driving working condition speed-time schedule, output battery system power-time schedule, such as New Europe Driving Cycle (NEDC), The Federal Urban Driving (FUDS) (2) cycle-shifted multiplier discharge and charging processes at various operating currents, such as Dynamic Stress Test (DST), Beijing Dynamic Stress Test (BJDST). In this paper, we use the working condition test data at different temperatures from the University of Maryland battery test dataset.

Figure 36.1 shows the speed-time diagram for the driving conditions of the electric vehicle and Fig. 36.2 shows the power-time diagram for the power cell under simulated driving conditions of the electric vehicle.

36.2.2 Segmentation

In this paper, we first segment multiple sets of vehicle driving condition speed-time-table data (US06, NEDC, Highway, FTP75), and also segment battery power-time under simulated dynamic conditions (FUDS, US06, DST, BJDST) of the power battery. The condition segmentation transforms the condition engineering into a process of inter-transfer between states and analyses the effect of the frequency of state changes on the battery simulation condition testing. In this regard, the length of time and division of the velocity–time data time segments are given by the following

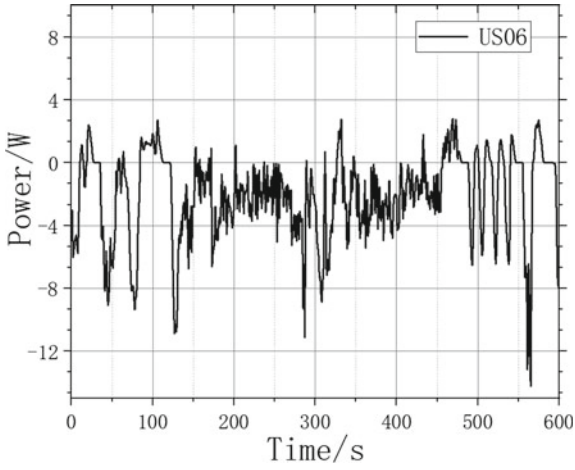

Fig. 36.1 Electric vehicle driving conditions US06 speed-time diagram

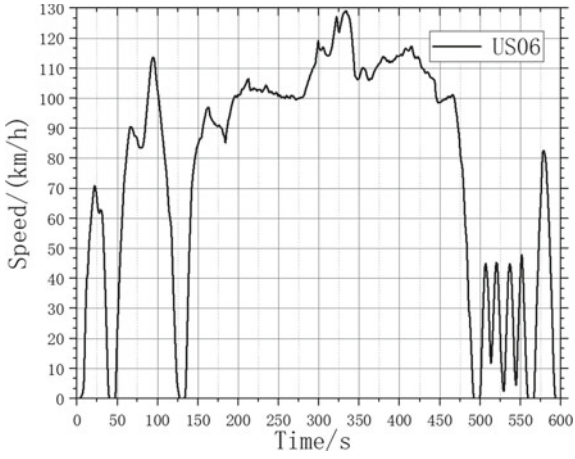

Fig. 36.2 Power battery unit power-time diagram under EV driving simulation

equations.

$$T = t_{end} - t_{start} \tag{36.1}$$

where T is the single state time length, t_{start} is the start time of that state and t_{end} is the end time of that state.

36.2.3 Feature Parameter Construction

The characteristic parameters of the analysed segments were constructed, and the segmented segments were statistically and analytically divided. Table 36.1 shows the selected driving conditions' feature parameters, which are mainly divided into the total time share of the fragment, the fragment speed and state transition frequency acceleration amount and the state transition frequency feature parameters.

Where the total segment time share includes uniform speed Travel time T_1, Acceleration travel time T_2, Braking time T_3, Idling time T_4 and start time T_5. Slice speed versus Amount of acceleration includes average speed $V_{average}$, Maximum velocity V_{max}, maximum acceleration a_{max} and maximum deceleration a_{break}. State transitions Frequency includes Start to accelerate, acceleration to constant speed, uniform to braking, acceleration to braking, brake to idle, braking to standstill. Frequency to time ratio of state transitions includes Start to accelerate f_1, Acceleration to constant speed f_2, Uniform to braking f_3, Acceleration to braking f_4, Brake to idle f_5, Braking to standstill f_6, Frequency to time ratio of state transitions r.

The total time share of selected simulated electric vehicle driving condition segments and state transition frequencies are calculated by (36.2) and (36.3) as follows.

$$f_i = \frac{n_i}{\sum_{j=1}^{6} n_j} (i = 1, 2, ..., 6) \tag{36.2}$$

$$T_i = \frac{\sum_{k=1}^{m} T_{k,i}}{\sum_{j=1}^{5} \sum_{k=1}^{m} T_{k,j}} (i = 1, 2, ..., n) \tag{36.3}$$

Table 36.1 Calculation of battery discharge and energy recovery operating conditions

	US06	BJDST	DST	FUDS
t_1	0.06	0.08	0.12	0.15
t_2	0.91	0.90	0.68	0.62
t_3	0.02	0.01	0.10	0.12
t_4	0.00	0.00	0.10	0.11
$P_{average}$	0.92	0.68	0.88	0.80
P_{max}	14.32	6.34	14.54	14.50
P_{cmax}	11.07	4.18	12.59	15.19
P_{dmax}	−16.38	−5.19	−13.16	−15.19
F_1	0.33	0.33	0.33	0.32
F_2	0.37	0.36	0.35	0.40
F_3	0.00	0.00	0.00	0.00
F_4	0.31	0.30	0.32	0.28
R	0.00	0.00	0.01	0.00

where f_i is the frequency of state transitions in the driving condition of the electric vehicle, n_i is the number of 6 state shifts in the driving condition process; T_i is the total time share of the electric vehicle driving condition state fragment; $T_{k,j}$ indicates the time length of the single state of the kth time slice in state j; m indicates the number of times state j appears. The selected simulated electric vehicle driving condition fragment speed and acceleration quantity calculation formula (36.4) is as follows.

$$V_{average} = \frac{1}{m_{\text{total}}} \sum_{i=1}^{m_{\text{total}}} \left(\frac{1}{T_i} \int_{t_{i,start}}^{t_{i,end}} V_i(t)dt \right) \tag{36.4}$$

where $V_{average}$ is the total average speed of the segments of the electric vehicle driving condition; m_{total} is the total number of time segments; T_i is the time length of a single state of segment i in the condition; t_{start} is the start time of the segment state and t_{end} is the end time of the segment state; V_i is the amount of time variation within the segment.

$$r = \frac{m_{total}}{T_{total}} \times 100\% \tag{36.5}$$

where r is the state transition frequency as a percentage of total time; m_{total} is the total number of time segments; T_{total} is the total length of the driving condition time state end time; V_i is the amount of time change within the segment.

The power battery power state change in the process of simulated power battery discharge and energy recovery is divided and the characteristic quantity is extracted, and the power battery discharge and energy recovery conditions are mainly divided into continuous discharge segment, continuous energy recovery segment and stationary segment.

Where the total segment time share includes Uniform discharge time t_1, Accelerated, Discharge time t_2, energy recovery time t_3 and resting time t_4. Slice power variables include Average output power $P_{average}$, Maximum output Power P_{max}, Maximum power climb rate P_{cmax} and Maximum power drop rate P_{dmax}. State transitions Frequency includes Standstill to acceleration F_1, Acceleration to energy recovery F_2, Uniform discharge to energy recovery F_3, Accelerated discharge to standstill F_4, Frequency to time ratio of state transitions R.

The total time share of the selected simulated power cell discharge and energy recovery segments and the state transition frequency are calculated in (36.5) and (36.6) as follows.

$$F_i = \frac{N_i}{\sum_{j=1}^{3} N_j} (i = 1, 2, 3) \tag{36.6}$$

$$t_i = \frac{\sum_{k=1}^{m} t_{k,i}}{\sum_{j=1}^{5} \sum_{k=1}^{m} t_{k,j}} (i = 1, 2, ..., n) \tag{36.7}$$

where F_i is the power battery state transition frequency, N_i is the power battery working condition power 5 state transfer times; t_i is the power battery working condition power state fragment total time share; $t_{k,j}$ indicates the state j in the kth time piece to maintain a state time length; m indicates the state j appear times. The average output power $P_{average}$ in the simulated power condition of the power cell is calculated as follows.

$$P_{average} = \frac{1}{m_{\text{total}}} \sum_{i=1}^{m_{\text{total}}} \left(\frac{1}{T_i} \int_{t_{i,start}}^{t_{i,end}} P_i(t)dt \right) \tag{36.8}$$

36.3 Principal Component Analysis and Battery Equivalent Circuit Model Construction

Let there be K working conditions, each with p characteristic parameters, denoted as $X = (x_1, x_2, ..., x_p)$. Let the mean value of the random variable X be μ and the covariance matrix $\sum$. After normalising the data in the working conditions by $(x_1 - \mu)/\sigma$ and normalising X, the covariance matrix $\sum$ of x is equal to its correlation coefficient matrix. The principal component is the problem of linearly combining p characteristic parameters. A linear transformation of X generates a new composite indicator, the principal component, denoted $y_1, y_2, \ldots, y_p$. The covariance matrix is used to find the eigenvalues $\lambda_1, \lambda_2, \ldots, \lambda_p$ ($\lambda_1 \geq \lambda_2 \geq \ldots \geq \lambda_p$) and the corresponding eigenvectors A as in (36.9).

$$A = \begin{bmatrix} a_{1,1} & a_{1,2} & \ldots & a_{1,p} \\ a_{2,1} & a_{2,2} & \ldots & a_{2,p} \\ \ldots & \ldots & \ldots & \ldots \\ a_{p,1} & a_{p,1} & \ldots & a_{p,p} \end{bmatrix} \tag{36.9}$$

Then each principal component of the characteristic parameters $x_1, x_2, \ldots, x_p$ after the orthogonal transformation can be expressed as (36.10)

$$\begin{cases} y_1 = a_{1,1}x_1 + a_{1,2}x_2 + \ldots + a_{1,p}x_p \\ y_2 = a_{2,1}x_1 + a_{2,2}x_2 + \ldots + a_{2,p}x_p \\ \ldots \\ y_p = a_{p,1}x_1 + a_{p,2}x_2 + \ldots + a_{p,p}x_p \end{cases} \tag{36.10}$$

where $y_1, y_2, \ldots, y_p$ are called the principal components, respectively.

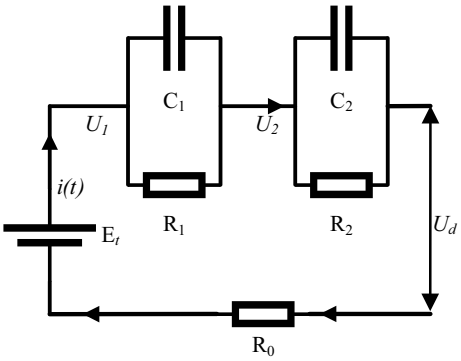

Fig. 36.3 Thevenin equivalent circuit model of the power cell

An equivalent circuit model is constructed [11], with the equivalent power cell unit as a second-order equivalent circuit. Figure 36.3 shows the power cell Thevenin second-order equivalent circuit model. R_0 is the internal resistance of the power cell; E_t is the open-circuit voltage potential; R_1 is the electrochemical polarisation internal resistance, R_2 is the concentration polarisation internal resistance; C_1 is the electrochemical polarisation capacitance, C_2 is the concentration polarisation capacitance; U_d is the measurable terminal voltage; U_1, U_2 are the battery polarisation internal resistance voltages and $i(t)$ is the real-time battery operating current.

The power cell unit model is built by Simulink. Figure 36.4 shows a schematic diagram of the Simulink equivalent circuit model of the power cell unit.

The HPPC test is carried out on the power cell, and the OCV-SOC curve and R_0, R_1, R_2, C_1 and C_2 equivalent circuit model parameters of the battery cell are identified by the HPPC condition. Finally, the current in various battery discharging and energy recovery conditions is used as model input to observe the error between the simulated voltage output and the actual observed voltage in the power cell simulation model,

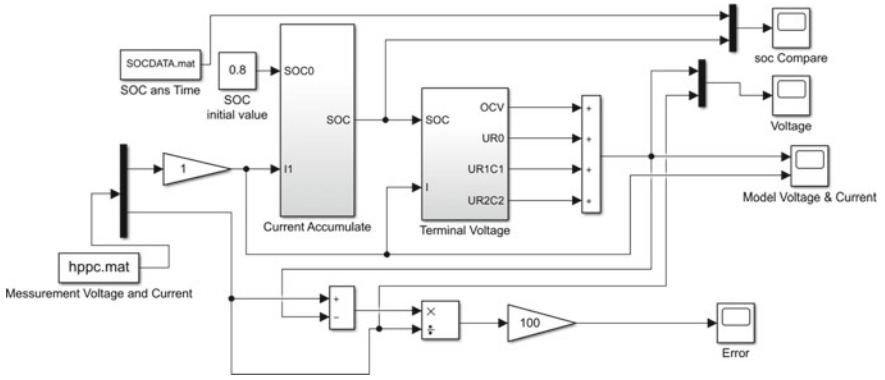

Fig. 36.4 Simulink equivalent circuit model of power battery unit

and the characteristic quantities with high contribution to the battery are compared with the error values.

36.4 Discussion

Multiple sets of vehicle speed-timeline data (US06, NEDC, Highway, FTP75) were segmented and the results of the selected driving condition segmentation feature parameters were calculated. Table 36.1 shows calculation of battery discharge and energy recovery operating conditions. Table 36.2 shows variation of response error of the simulated cell model under different operating conditions. Table 36.3 shows battery discharging and energy recovery working condition principal component score table.

Table 36.2 Variation of response error of the simulated cell model under different operating conditions

Simulated working conditions	Average absolute error of voltage simulation %	Voltage simulation maximum absolute error %	Root mean square error of voltage simulation %
US06	2.41	18.20	3.16
BJDST	2.26	7.06	8.71
DST	1.48	19.48	2.79
FUDS	3.21	19.91	4.70

Table 36.3 Battery discharging and energy recovery working condition principal component score table

Principal component number	Eigenvalue	Contribution	Cumulative contribution
1	6.63	0.51	0.51
2	4.29	0.33	0.84
3	2.08	0.16	1
4	3.87×10^{-16}	2.98×10^{-17}	1
5	3.30×10^{-16}	2.54×10^{-17}	1
6	2.10×10^{-16}	1.63×10^{-17}	1
7	1.06×10^{-16}	8.19×10^{-17}	1
8	-7.47×10^{-17}	-5.74×10^{-17}	1
9	-1.38×10^{-16}	-1.06×10^{-17}	1
10	-2.24×10^{-16}	-1.73×10^{-17}	1
11	-2.45×10^{-16}	-1.89×10^{-17}	1
12	-4.94×10^{-16}	-3.80×10^{-17}	1
13	-1.15×10^{-16}	-8.87×10^{-17}	1

The analysis of the battery discharge and energy recovery working condition principal component score table, with the battery simulation model under this discharge and energy recovery working condition, shows that the prediction error of the power battery model is positively correlated with the high contribution of the characteristic parameters in the principal component analysis of the battery discharge and energy recovery working condition that it is subjected to.

36.5 Conclusion

In this paper, we select and segment the data of various types of electric vehicle driving conditions and the simulated working condition data used to simulate the power battery, extract the relevant characteristic parameters in the working condition data, and analyse the simulated working condition data of the power battery and the electric vehicle driving condition data by using the principal component analysis method. The typical working conditions of the simulated power battery working condition data and the electric vehicle driving working condition US06 are selected to analyse and compare the principal components of the two types of working conditions and to analyse the influence of the working conditions on the construction of the power battery model.

Acknowledgements This paper is one of the stage results of the Guangdong Key Areas R&D Project Power Battery System Testing and Evaluation Technology Research (2019B090908003). The authors also thanks to the Center for Advanced Life Cycle Engineering (CALCE) at the University of Maryland for providing us with an open-source dataset of power cells for our services.

References

1. J. Brady, M. O'Mahony, Development of a driving cycle to evaluate the energy economy of electric vehicles in urban areas. Appl. Energy **177**, 165–178 (2016)
2. GB/T 38146.1-2019, Driving conditions for automobiles in China Part 1: Light-duty vehicles (2019)
3. GB/T 38146.2-2019, Driving conditions for automobiles in China Part 2: Heavy commercial vehicles (2019)
4. China Automotive Technology Research Center, The Eighteenth Research Institute of China Electronics Technology Group Corporation, Tianjin Lishen Battery Co. Lithium-ion power battery packs and systems for electric vehicles Part 2: Test procedures for high-energy applications. J. GB/T 31467.2-2015:24 (2015)
5. X.-Y. Song, C.-L. Wang, Electric vehicle power system modeling based on joint CarSim/Simulink simulation. Agric. Equip. Veh. Eng. **58**, 100–105 (2020)
6. F. Sun, X. Meng, C. Lin, Research on dynamic test conditions of electric vehicle power battery. J. Beijing Univ. Technol. **30**, 297–301 (2010)
7. H. Gong, Y. Zou, Q. Yang, Generation of a driving cycle for battery electric vehicles: a case study of Beijing. Energy **150**, 901–912 (2018)

8. S. Shi, N. Lin, Y. Zhang, Research on Markov property analysis of driving cycles and its application. Transp. Res. Part D-Transp. Environ. **47**, 171–181 (2016)
9. E. Chemali, P.J. Kollmeyer, M. Preindl, State-of-charge estimation of Li-ion batteries using deep neural networks: a machine learning approach. J. Power Sources **400**, 242–255 (2018)
10. F. Wang, Z. Wang, S. Xu, Complex operating conditions testing and simulation of integrated environmental power battery systems. Power Technol. **40**, 527–528+579 (2016)
11. K.X. Wei, C. Qiaoyan, State estimation of lithium-ion power battery based on adaptive traceless Kalman filter algorithm. Chin. J. Electr. Eng. **34**, 445–452 (2014)